Royal Netherlands
Meteorological Institute
Ministry of Infrastructure and the Environment

TROPOMI ATBD of the UV aerosol index

TROPOMI

sentinel-5p

Document approval record

	digital signature
prepared:	
checked:	M. Penning-de Vries, M. Sneep, G. Tilstra, O. Bouchard, J. Fischer, and R. Martin
approved PM:	
approved PI:	

Document change record

issue	date	item	comments
0.0.1	2012-09-10	All	Initial version.
0.0.2	2012-09-25	All	Updated with feedback from KNMI Level-2 team.
0.1.0	2012-09-27	-	Released for first review by Level-2 Working Group.
0.1.1	2012-11-16	All	Updated with feedback from aerosol science verification team. Document number changed from S5P-KNMI-L2-0115-RP to S5P-KNMI-L2-0006-RP.
0.2.0	2012-11-16	-	Released for first review by ESA.
0.3.0	2013-06-04	All	AAI and ALH ATBDs split into separate documents; Updated with feedback from ESA; Released for internal review.
0.5.0	2013-06-21	All	Updated with feedback from internal review; Released for ESA external review.
0.9.0	2013-12-03	All	Updated with feedback from ESA external review; Released for further ESA review.
0.10.0	2014-04-15	All	Updated to address outstanding RIDs from ESA external review; Released for further ESA review
0.11.0	2014-09-30	All	Updated to finalize outstanding RIDs and issues raised during most recent L2CDR; Released for ESA review
0.13.0	2015-09-16	All	Product name updated from AI to UVAI; Content updated to reflect most recent version of IODD; Released for S5PVT review
1.0	2016-02-03	All	References updated and all text updated to reflect comments from internal review.
1.1	2018-06-15	Section 4.2.1.1	Description of spectral sampling effect correction added.

Contents

1   Introduction to this document

1.1   Identification

This document, identified as S5P-KNMI-L2-0008-RP, is the Algorithm Theoretical Basis Document (ATBD) for the TROPOMI UV aerosol index. It is part of a series of ATBDs describing the TROPOMI Level-2 products.

1.2   Purpose and objective

The purpose of this document is to describe the current implementation and the theoretical basis of the aerosol index Level-2 algorithm. The document is maintained during the development phase and the lifetime of the data products. Updates and new versions are foreseen if there are changes to the algorithm.

1.3   Document overview

Section 2 lists applicable and reference documents within the S5P/TROPOMI project. Section 3 gives a list of terms, abbreviations and symbols that are specific for this document. Section 4 discusses the UV Aerosol Index (UVAI). Section 5 presents the validation plan for the TROPOMI aerosol products. Section 6 provides general conclusions and an outlook. Finally, Section 7 lists references to peer-reviewed papers and other scientific publications.

Readers interested in reading more about the Aerosol Layer Height (ALH) algorithm should refer to the ATBD for ALH.

1.4   Acknowledgements

2 Applicable and reference documents

2.1 Applicable documents

[AD01] Science Requirements Document for TROPOMI, Volume I: Mission and Science Objectives and Observational Requirements;
source: KNMI; **ref:** RS-TROPOMI-KNMI-017; **issue:** 2.0; **date:** 2008-10-30

2.2 Reference documents

[RD01] Terms, definitions and abbreviations for TROPOMI L01b data processor;
source: KNMI; **ref:** S5P-KNMI-L01B-0004-LI; **issue:** 3.0.0; **date:** 2013-11-08

[RD02] Terms and symbols in the TROPOMI Algorithm Team;
source: KNMI; **ref:** SN-TROPOMI-KNMI-049; **issue:** 0.0.2; **date:** 2012-08-28

[RD03] Algorithm theoretical basis document for the TROPOMI L01b processor;
source: KNMI; **ref:** S5P-KNMI-L01b-0009-SD; **issue:** 6.0.0; **date:** 2015-09-22

[RD04] TROPOMI Instrument Performance Analyses Report;
source: DutchSpace; **ref:** TROP-DS-0000-RP-0060; **issue:** 6.0; **date:** 2013-01-16

[RD05] TROPOMI cloud retrieval algorithm concept;
source: KNMI; **ref:** RP-TROPOMI-KNMI-048; **issue:** 1.2; **date:** 2010-10-11

[RD06] DISAMAR: Determining Instrument Specifications and Analyzing Methods for Atmospheric Retrieval, Algorithms and background;
source: KNMI; **ref:** RP-TROPOMI-KNMI-066; **issue:** - ; **date:** 2012-01-24

[RD07] DISAMAR: Determining Instrument Specifications and Analyzing Methods for Atmospheric Retrieval, User Manual;
source: KNMI; **ref:** RP-TROPOMI-KNMI-104; **issue:** - ; **date:** 2012-02-08

[RD08] Sentinel 5 precursor/TROPOMI KNMI and SRON level 2 Input Output Data Definition;
source: KNMI; **ref:** S5P-KNMI-L2-0009-SD; **issue:** 4.0.0; **date:** 2015-11-02

[RD09] Input/Output data specification for the TROPOMI level 01b data processor;
source: KNMI; **ref:** S5P-KNMI-L01B-0012-SD; **issue:** 5.0.0; **date:** 2015-09-22

[RD10] TROPOMI Instrument and Performance Overview;
source: KNMI; **ref:** S5P-KNMI-L2-0010-RP; **issue:** 0.10.0; **date:** 2014-03-15

[RD11] S5P/TROPOMI L2 Support products;
source: KNMI; **ref:** S5P-KNMI-L2-0125-TN; **issue:** 0.13.0; **date:** 2015-09-25

[RD12] S5P/TROPOMI Static input for Level 2 processors;
source: KNMI; **ref:** S5P-KNMI-L2CO-0004-SD; **issue:** 3.0.0; **date:** 2015-02-27

2.3 Electronic references

3   Terms, abbreviations and symbols

Terms, abbreviations and symbols that are used within the TROPOMI Level-2 project are described in [RD01] and [RD02]. Terms, abbreviations and symbols that are specific for this document can be found below.

3.1   Terms

height	vertical height, either in units of Pa (pressure) or in units of m (altitude)

3.2   Abbreviations

AI	Aerosol Index
AAI	Absorbing Aerosol Index
ACAM	Airborne Compact Atmospheric Mapper
AERONET	Aerosol Robotic Network
ALH	Aerosol Layer Height
CAMS	Copernicus Atmosphere Monitoring Service
DISAMAR	Determining Instrument Specifications and Analyzing Methods for Atmospheric Retrieval
ECMWF	European Centre for Medium-Range Weather Forecasts
FRESCO	Fast Retrieval Scheme for Clouds from the Oxygen A band
GOME(-2)	Global Ozone Monitoring Experiment
GMES	Global Monitoring of the Environment and Security
HITRAN	High Resolution Transmission
LABOS	layer-based orders of scattering
LER	Lambert-equivalent reflector
LUT	look-up table
OMAERO	OMI/Aura Aerosol Optical Thickness & Aerosol types
OMI	Ozone Monitoring Instrument
OMPS	Ozone Mapping & Profiler Suite
RT	radiative transfer
SCI	Scattering Index
SCIAMACHY	Scanning Imaging Absorption Spectrometer for Atmospheric Chartography
SeaWiFS	Sea-viewing Wide Field-of-view Sensor
S5P	Sentinel-5 Precursor
Suomi NPP	Suomi National Polar-orbiting Partnership
TOMS	Total Ozone Mapping Spectrometer
TROPOMI	Tropospheric Monitoring Instrument
UV	ultraviolet
UVAI	ultraviolet aerosol index
VIIRS	Visible Infrared Imaging Radiometer Suite

3.3   Symbols

ω_0 single scattering albedo [-]

τ_0 (sometimes: τ)   aerosol or cloud optical thickness [-]

4   UV aerosol index

4.1   Introduction

The Aerosol Index (AI) is a well-established data product that has been calculated for several different satellite instruments spanning a period of more than 30 years. The Aerosol Index described in this ATBD is explicitly named the UVAI since it is based on spectral contrast in the ultraviolet (UV) spectral range for a given wavelength pair, where the difference between observed and modeled reflectance results in a residual value. When this residual is positive it indicates the presence of UV-absorbing aerosols, like dust and smoke, and is often referred to as the Absorbing Aerosol Index (AAI). Clouds yield near-zero residual values and negative residual values can be indicative of the presence of non-absorbing aerosols. Unlike satellite-based aerosol optical thickness measurements, AAI can also be calculated in the presence of clouds so that daily, global coverage is possible. This is ideal for tracking the evolution of episodic aerosol plumes from dust outbreaks, volcanic ash, and biomass burning.

4.1.1   Product description

The relatively simple calculation of the Aerosol Index is based on wavelength dependent changes in Rayleigh scattering in the UV spectral range where ozone absorption is very small. For a given wavelength pair a ratio is calculated from measured top of the atmosphere (TOA) reflectance and pre-calculated theoretical reflectance for a Rayleigh scattering-only atmosphere and results in a residual value. Positive values of this residual indicate the presence of UV-absorbing aerosol. The UVAI is dependent upon aerosol layer characteristics including aerosol optical thickness (τ_0), aerosol single scattering albedo (ω_0), aerosol layer height (ALH), and the underlying surface albedo. The UVAI is a robust calculation that is well proven based on years of data, where the major strengths include speed of calculation, global coverage, ease of use, and the potential for creation of long-term climate data records. The terms AI, UVAI and AAI will all be used in this document. AI will used in this ATBD as a collective term referring to all current and historical measurements of the aerosol index as derived from several different satellite instruments. UVAI refers to the S5P/TROPOMI product described in this ATBD that includes both positive and negative residual values. The AAI refers to the final interpretation of the UVAI data where positive values are evaluated to determine presence of strongly absorbing and/or elevated aerosol layers. It should be noted that the Aerosol Index verification algorithm will be explicitly calculating what is known as the Scattering Index (SCI) (Penning de Vries, et al., 2009).

4.1.2   Heritage

The AI is a widely used and well-tested aerosol data product spanning more than 30 years and has been calculated for a variety of satellite instruments including the Total Ozone Mapping Spectrometer (TOMS) for both Nimbus-7 and Earth Probe (EP) instruments, the Global Ozone Monitoring Experiment (GOME), and the following GOME-2, the Ozone Monitoring Instrument (OMI) and the Scanning Imaging Absorption Spectrometer for Atmospheric Chartography (SCIAMACHY). The AI was first calculated as a correction for the presence of aerosols in column ozone measurements made by the TOMS instruments (Herman et al., 1997; Torres et al., 1998), because it was observed that ozone values were too high in typical regions of aerosol emission and transport.

The first TOMS mission began measuring ozone on the Nimbus-7 platform in 1978 and the eventual aerosol correction product came out of the successor TOMS-EP which spanned the period of 1996 to 2005. The satellite instruments that have measured AI, the respective platforms, years of data availability, and the wavelength pair used for AI calculation are summarized in Table 4-1. The majority of these instruments shown in Table 4-1 use the TOMS (Nimbus-7) heritage 340/380 nm wavelength pair. Exceptions include the 331/360 nm pair used by TOMS-EP and the 354/388 nm pair used by KNMI-developed OMAERO AI. It is the aim for the TROPOMI mission to choose wavelength pairs within one channel and continue the multi-decadal heritage measurement record by using the 340/380 nm pair. To continue the OMI data record and for comparison purposes UVAI will also be calculated for the 354/388 nm pair as the computational effort is minimal.

Table 4-1. Satellite instruments and related wavelength pairs.

Instrument / Platform	Wavelength Pair (nm)	Years of Available Data
TOMS / Nimbus-7	340 / 380[†]	1978 – 1993
GOME / ERS-2	340 / 380	1995 – 2003

TOMS / Earth Probe	331 / 360	1996 – 2005
SCIAMACHY / Envisat	340 / 380	2002 – 2012
OMI / Aura	354 / 388	2004 – present
GOME-2 / MetOp	340 / 380	2007 – present
OMPS / Suomi NPP	336 / 377	2012 – present

[†]*Note that the current TOMS data (v8) uses the 331/360 wavelength pair.*

4.1.3   Product requirements

The UVAI has few requirements as it depends on no a priori information and little external information is needed for calculation. As described by the TROPOMI Science Requirements Document ([AD01]) the experience from TOMS and OMI dictates that the UVAI must have an accuracy of 0.25 to distinguish the presence of aerosol from the background. Well-calibrated, error-characterized radiances are of greatest importance for the calculation of the UVAI. Error requirements for the radiance are discussed in more detail in Section 4.4.1. It is also a requirement to have both wavelengths in the same spectral channel to avoid inter-channel deviation. This is the primary reason why the KNMI OMI AI wavelength pair of 354/388 nm differed from the standard 340/380 nm pair—to ensure that both wavelengths were within the same OMI visible (VIS) channel. If the wavelengths are not located in the same channel, imperfect co-alignment and calibration differences will lead to apparently random and systematic biases in the calculated AI. Further, wavelengths must be chosen in the UV taking into consideration the proximity of Fraunhofer lines, interfering absorbers (i.e. ozone), and the wavelength dependent behavior of surface albedo at and between the defined wavelength pair (for the latter see also Section 4.4.2).

4.1.4   Overview of retrieval methods

As stated earlier, the UVAI consists of a calculation of a ratio that yields a residual value and as such the UVAI is not a classical retrieval. Calculation of the UVAI relies upon measured radiance in terms of reflectance, theoretical reflectance from an atmosphere with only Rayleigh scattering stored in a pre-computed look-up table (LUT), and upon the assumption that the scene surface behaves as a Lambert Equivalent Reflector (LER; Dave and Mateer, 1967). An overview of the UVAI calculation process is given in Figure 4-1.
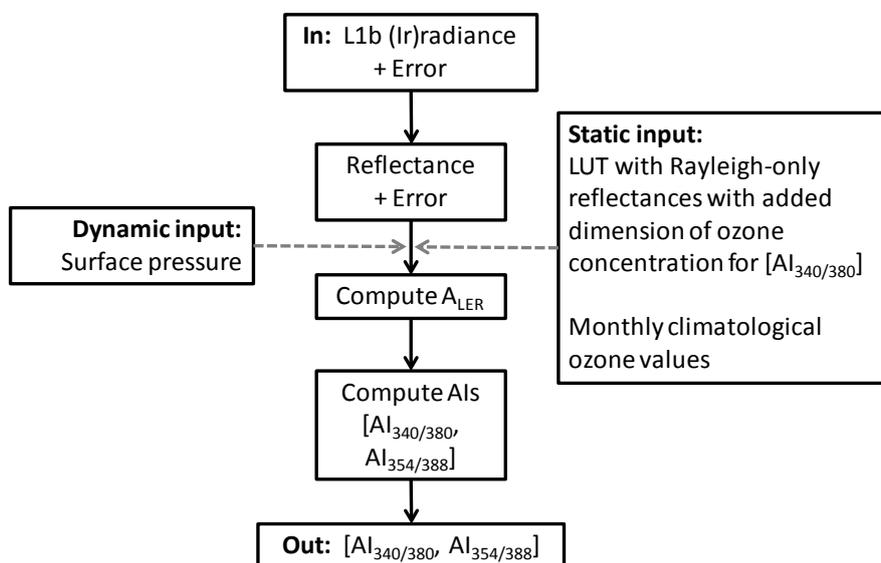

Figure 4-1. Flow chart overview of the calculation of aerosol indices.

4.1.5   Foreseen update approach

Few updates are foreseen for the UVAI as it will be calculated keeping in mind the benefits of heritage and a long-term climate record data set. Updates to the wavelength choice could be applied if necessary based on the quality of the measured reflectance and instrument characteristics. The dependency of UVAI on knowledge of surface albedo and behavior will continue to be monitored and quantified (see Section 4.4.2) and could lead to slight modification of UVAI calculation methods as well as error characterization and reporting.

4.1.6   Product User Community

The AI has a broad user community, which utilize the AI for both scientific and operational purposes. Because the AI is available in near-real-time (NRT) with daily, global coverage from multiple satellite platforms it is well-suited for verifying the presence of episodic aerosol plumes including volcanic ash (Seftor et al., 1997; Krotkov et al., 1999), biomass burning smoke (Hsu et al., 1996) and desert dust outbreaks (Chiapello et al., 1999). The AI can help meet a range of GMES user community needs described in Ingmann et al., (2012) including long-term monitoring of the presence of radiatively important UV-absorbing aerosols as well as NRT volcanic ash plume monitoring.

The AI can also be used in conjunction with other datasets to utilize the information contained about aerosol type or height as has been shown in Hsu et al. (1999), given external information about AOT from AERONET. As demonstrated by Wang et al. (2011), the FRESCO algorithm can be used to retrieve aerosol layer height for optically thick aerosol layers. When using AI data in combination with FRESCO-derived aerosol layer height, de Laat et al. (2012), showed that information could be derived about the SSA of the aerosol layer. Thus, the AI can be used in scientific, research applications when combined with other AOT and/or ALH datasets. With respect to TROPOMI, AI data can be used together with the ALH product to better interpret aerosol type. Since TROPOMI will be flying in close formation to VIIRS, AOT and information about fine versus coarse mode aerosol from VIIRS can be used with AI data to develop a broad aerosol typing scheme. Such a product would be considered a research product and would not therefore be included in the operational production of UVAI.

4.2   Algorithm description and computation method

In this section a more detailed description of the methods used for computing the UVAI are described. The UVAI is not a classical satellite retrieval as no spectrum is fitted. Rather, based on a series of inputs including the satellite measured Earth radiance and pre-computed LUT values, the UVAI is calculated. Here the computation of the AI is derived highlighting the assumption of a LER surface and that LER is assumed to be equal at both wavelengths. The AI depends on measured radiances but is presented and derived here in terms of reflectance, where reflectance (R) is given in Eq. 4-1 by:

$$R(\lambda) = \frac{\pi I(\lambda)}{\cos(\theta_0) \cdot E_0(\lambda)} \,. \qquad \text{Eq. 4-1}$$

$I(\lambda)$ is the radiance reflected by Earth (atmosphere and surface) to the sensor, θ_0 is the solar zenith angle and $E_0(\lambda)$ is the solar irradiance. Here the only argument given is the wavelength, but the reflectance depends on other parameters, given in the Eq. 4-2 and Table 4-2 below, where $A_s(\lambda)$ is the albedo of the surface:

$$R(\lambda, A_s(\lambda)) = R_a(\lambda) + \frac{A_s(\lambda)T(\lambda)}{1 - A_s(\lambda)s(\lambda)} \qquad \text{Eq. 4-2}$$

.

Table 4-2. Terms used in the definition and derivation of the AI

$R(\lambda, A_s(\lambda))$	Is the reflectance of the combined atmosphere-surface system
$R_a(\lambda)$	Is the reflectance of the atmosphere if the surface is perfectly black, $A_s(\lambda) = 0$
$A_s(\lambda)$	Is the albedo of the surface, which is assumed to be a Lambertian (isotropic) reflector

$T(\lambda)$	Is the transmittance of the atmosphere, a measure for the probability that photons travel through the atmosphere, are reflected by a surface with unit albedo, and travel back to the sensor. Reflections by the atmosphere back towards the surface are ignored here.
$s(\lambda)$	Is the spherical albedo of the atmosphere for illumination at its lower boundary. $1/[1-A_s(\lambda)s(\lambda)]$ is the sum of a geometrical series accounting for the reflections between the atmosphere and the surface.

In general, the reflectance depends on the wavelength, the surface albedo, the solar zenith angle, the viewing zenith angle, the azimuth difference between the incident sunlight and the scattered light, ozone column (and possibly other trace gases), the surface pressure and the composition of the atmosphere (presence and vertical location of cloud and/or aerosol layers). $R_a(\lambda)$, $T(\lambda)$ and $s(\lambda)$ are known from interpolation from a look-up table for a given geometry and surface pressure.

When calculating the aerosol index a comparison is made between the spectral reflectance of the atmosphere-surface system and an atmosphere consisting purely of molecules. Further, it is assumed that the surface behaves as a LER surface, so that the reflectance in Eq. 4-2 can be rewritten as:

$$R(\lambda, A_{LER}(\lambda)) = R_{Ray}(\lambda) + \frac{A_{LER}(\lambda)T_{Ray}(\lambda)}{1 - A_{LER}(\lambda)s_{Ray}(\lambda)}$$

Eq. 4-3

,

where $A_{LER}(\lambda)$ is the real surface albedo if there are no clouds or aerosol present. It should be noted that $A_{LER}(\lambda)$ can take on negative values as it is a not a true surface albedo term. The subscript Ray in Eq. 4-3 refers to a purely molecular atmosphere for which the scattering is described by Rayleigh scattering. The Rayleigh terms (R_{Ray}, T_{Ray}, s_{Ray}) are provided by interpolation of a look-up table. Given that the measured reflectance value at wavelength λ_1 is known then Eq. 4-3 can be used to solve for the LER:

$$A_{LER}(\lambda_1) = \frac{R_{meas}(\lambda_1) - R_{Ray}(\lambda_1)}{T_{Ray}(\lambda_1) + s_{Ray}(\lambda_1)[R_{meas}(\lambda_1) - R_{Ray}(\lambda_1)]}$$

Eq. 4-4

.

A general expression for the aerosol index can be given as such:

$$AI = 100 \cdot \log_{10}\left(\frac{R_{meas}(\lambda_2)R_{calc}(\lambda_1, A_{LER}(\lambda_1))}{R_{meas}(\lambda_1)R_{calc}(\lambda_2, A_{LER}(\lambda_2))}\right)$$

Eq. 4-5

.

Here, the key assumption is made that $A_{LER}(\lambda_1) = A_{LER}(\lambda_2)$. The reference wavelength is set here to be the longer of the two so that, $R_{meas}(\lambda_2) = R_{calc}(\lambda_2, A_{LER}(\lambda_2))$. Using A_{LER} at the reference wavelength, AI can be rewritten from the general expression in Eq. 4-5 and reduced to:

$$AI = 100 \cdot \log_{10}\left(\frac{R_{\text{calc}}(\lambda_1, A_{LER}(\lambda_2))}{R_{\text{meas}}(\lambda_1)} \right) \qquad \text{Eq. 4-6}$$

Thus, the aerosol index relies upon measured reflectance at the shorter wavelength for a defined wavelength pair and the calculated Rayleigh reflectance given a LER surface assumed to be equal for both wavelengths. The Rayleigh reflectance and related radiative transfer terms (Table 4-2) are stored in a pre-computed LUT for both wavelengths. The dimensions of the LUT include surface pressure, solar zenith angle, viewing zenith angle, relative azimuth angle in terms of a Fourier expression, and Chandrasekhar treatment of surface albedo [RD05] (See also Appendix). Ozone column concentration is included as an additional dimension for calculation of UVAI with the 340/380 nm wavelength pair [See further detail in Sections 4.3.2 and 4.4.4].

4.2.1 Algorithm Input

Detailed description of all dynamic, semi-dynamic, and static input data is given in [RD08], [RD12].

4.2.1.1 Dynamic input

The dynamic data needed for calculating the aerosol index is summarized in Table 4-3. In order to remove the effects of the spectral sampling on the output, a triangular weighting function is applied to the input spectrum. The base of the triangular weighting function has a width of 2 nm.

Table 4-3. Dynamic input for aerosol index.

Name/Data	Symbol	Unit	Source	Pre-process needs	Backup if not available	Comments
S5P level 1B Earth Radiance Band 3	R_{meas}	Photons/sec/m2/nm	S5P level 1B product	Per ground pixel	no retrieval	
S5P level 1B Solar Irradiance UVN band	$E_0(\lambda)$	Photons/sec/m2/nm	S5P level 1B product	--	previous measurement	
ECMWF surface pressure fields from forecast		Pa	ECMWF	Spatial grid: 1° x 1° or finer	previous day forecast	3-hour interval forecast data
ECMWF total ozone column		Dobson units [DU]	ECMWF (CAMS)	Spatial grid: 1° x 1° or finer	previous day forecast; TOMS V8 climatology	3-hour interval forecast data

4.2.1.2 Static input

The static data needed for calculating the aerosol index is summarized in Table 4-4.

Table 4-4. Static input for aerosol index.

Name/Data	Symbol	Unit	Source	Pre-process needs	Backup if not available	Comments
LUT_AAI		--	S5P level 2 algorithm and process file		--	(See Appendix)
Surface elevation		m	Geopotential height used by ECMWF	Spatial grid: 0.25° x 0.25° or finer		

4.2.2   Algorithm Output

Detailed description of algorithm output including file formatting is given in [RD08]. Output files are organized into two sections consisting of metadata and the product. The data product consists of 11 data fields and support data where the latter is divided into three categories: Detailed Results, Geolocations, and Input Data. The input data is described in the previous section (4.2.1). Variables and dimensions common to all products including coordinate variables, geolocation fields, and common product fields are described in [RD08]. A summary of the output specific to the aerosol index algorithm is summarized in Table 4-1. Additionally, the detailed results portion of the support data contains eight aerosol index specific products including scene albedo at the reference wavelength and measured and calculated reflectances for each wavelength of the two wavelength pairs. Details of these fields including aerosol index specific quality assurance statistics in the metadata are given in [RD08].

Table 4-5. Algorithm output for aerosol index

Name/Data	Symbol	Unit	Description	Data type per pixel	Number of values	Comments
aerosol_index_340_380			AI for 340/380 nm	Float	1	
aerosol_index_354_388			AI for 354/388 nm	Float	1	

4.3   Feasibility

The long heritage of the AI deems that the feasibility of this product is very high, as the computational methods are based upon well-tested and proven techniques that have been implemented and improved in conjunction with six different satellite instruments. Additionally, the low computational effort, no need of a priori information and little auxiliary data means that the UVAI is a highly feasible data product. It is expected that the UVAI will be calculated for all available pixels with no implementation of a spatial data selection approach. UVAI will be available in near real-time (NRT).

4.3.1   Estimated computational effort and robustness

The estimated computation effort for UVAI is low. This effort is based on the following steps: 1) read in necessary data including L1B radiances, satellite-sun geometry, and auxiliary surface pressure data; 2) interpolate the LUT containing pre-computed Rayleigh reflectance using the satellite-sun geometry and the surface pressure data; 3) computation of the UVAI using measured L1B radiances in terms of reflectance and the Rayleigh reflectance. The LUT will differ in structure to that used for OMI by using with a larger range of surface pressures to allow for smoother interpolation based on surface height, Fourier expansion terms for the relative azimuth angle, and a Chandrasekhar treatment for surface albedo [RD05] (See also Appendix). The size of the LUT is not expected to exceed 100 MB (currently 21 MB file size, 32 MB in memory) [RD08]. Using DISAMAR, simulated UVAI calculations take between 1-3 seconds depending on viewing geometry [RD06], [RD07]. However, when a LUT is used and measured radiances are read in rather than simulated it is expected to be a factor of 100 faster. Since the UVAI is a very robust calculation, it is not subject to issues of non-convergence that can be problematic for other retrieved data products. The UVAI retrieval algorithm is not iterative and therefore runs in constant time. The total run time is proportional to the number of ground pixels. Errors and warnings in UVAI data processing typically only arise due to quality issues with L1B radiances and extreme viewing geometries where the latter yields anomalously high UVAI values. UVAI data is typically used for solar zenith less than 60°. Although reliability is decreasing with SZA, UVAI will be calculated up for VZA up to 78° and for SZA up to 88°.

4.3.2 Auxiliary information needs

The UVAI needs very little auxiliary information for computation of the data product. All auxiliary data mentioned in this section is further described in [RD08]. Surface pressure is essential however, for the interpolation of the LUT containing pre-computed Rayleigh reflectance. The strong non-linear dependence of AI on surface pressure is described in De Graaf et al., (2005). The ECMWF 3-hour interval forecast product will be used for the surface pressure dataset. Additionally, total ozone column concentration from the ECMWF 3-hour interval forecast will be used for calculation of $AI_{340/380}$ where ozone absorption has a much greater effect than on $AI_{354/388}$ [See Section 4.4.4]. Extra information not needed for computation of UVAI but useful for the creation of addition of flags helpful for the interpretation of UVAI include surface type (ocean, coastal or land), snow and ice cover. The fast NRT KNMI cloud mask product will likely be included as an AI flag. Such a cloud flag can be used in combination with the UVAI data to indicate the presence of absorbing aerosol above cloud layers. An additional cirrus flag, likely provided by re-gridded VIIRS data, would be desirable for a non-operational research UVAI data product because absorbing aerosol as detected by UVAI is still discernable in the presence of cirrus.

4.3.3 Product description and size estimate

The UVAI product contains eleven data fields, geolocation fields as well as metadata, where geolocation field and metadata are further described in [RD08]. Geolocation fields include such parameters as sun-satellite geometry, latitude, longitude, time, and satellite altitude. Data fields will include UVAI for two wavelengths pairs, namely $AI_{340/380}$ and $AI_{354/388}$, surface pressure, terrain height and reflectivity, processing and measurement quality flags, instrument configuration parameters, and cloud flags including cloud fraction and/or cloud pressure, and flags for surface snow and ice cover. Production of two wavelength pairs for UVAI will maximize the opportunity to combine existing AI data records like that from OMI and SCIAMACHY and allow for continued study of how to best compute AI by minimizing errors and interferences. The error and sensitivity analysis presented in Section 4.4 has largely been carried out for both wavelength pairs to highlight the differences, strengths and weaknesses of each. The processing and measurement flags will be based on L1B defined quality level which takes into account the quality of each spectral channel and each ground pixel, where the latter includes important flags addressing solar eclipse for which UVAI must be screened [RD09]. An additional field with a simple estimate of error in UVAI based on the L1B radiance data product for the amount of statistical and systematic error in the measured spectral radiance will also likely be included in the UVAI data product.

The TROPOMI UVAI data files will contain only UVAI and related information. Based on the TROPOMI pixel size of 7x7 km at nadir with assumed orbit dimensions of 320 x 3300 pixels (across-track x along-track), the estimated file size for the UVAI output product including metadata is 110MB [RD08].

4.4 Error analysis

As UVAI is a qualitative measure of the presence of aerosols, it is essential to use simulations to assess UVAI dependencies and to separate these effects from errors in the calculation of UVAI. DISAMAR is an optimal estimation based radiative transfer scheme which employs layer-based orders of scattering (LABOS) and the HITRAN spectral database [RD07]. DISAMAR takes polarization into account. Simulations of the UVAI have been carried out to test the effect of various types of errors on the precision and accuracy of the UVAI. The UVAI is simulated in DISAMAR by specifying a wavelength pair, measurement characteristics including signal-to-noise ratio, prescribing aerosol layer(s), surface properties, and ozone concentration. The UVAI is then calculated using the method described in Section 4.2. These tests in DISAMAR were carried out for a single aerosol layer with an τ_0 of 1.0 located between 80000-70000 Pa with an underlying surface albedo of 0.05. The layer consists of "strongly absorbing", small spherical particles where the optical properties are defined according to types described in the context of the Aerosol-CCI project in Table 4-7. (De Leeuw et al., 2011). The experiments were carried out for UVAI using both 340/380 nm and 354/388 nm wavelength pairs and in the discussion that follows will be hereafter referred to as $AI_{340/380}$ and $AI_{354/388}$ respectively.

4.4.1 Instrument errors

The effects on UVAI due to simple offset errors in measured radiance (both additive and multiplicative) were tested using DISAMAR. The results for these tests are shown and discussed and may be representative of the type of error that will be provided by the L1B data product and used to create a L2 estimate of UVAI error [See Section 4.3.3]. There are several publications which extensively address the role that calibration issues can play in the correction of AI datasets (de Graaf and Stammes, 2005; de Graaf et al., 2005; Tilstra et al., 2012).

Simple offsets are defined in DISAMAR as additive and multiplicative offsets in percent for simulated and measured radiance and/or irradiance as follows,

$$L_{withOffset}(\lambda) = L_{withoutOffset}(\lambda) * (1.0 + Offset_{mul}/100) + L_{withoutOffset}(\lambda_{start}) *$$
$$(1.0 + Offset_{mul}/100) * Offset_{add}/100$$

Eq. 4-7

,

where L is radiance and λ is the wavelength in Eq. 4-7. The simple offsets led to biases in UVAI. The results for simulations with additive-only, multiplicative-only, or both in the irradiance and/or radiance are shown in Figure 4-2 and Figure 4-3. The biases are much smaller for $AI_{354/388}$ (Figure 4-3) than for $AI_{340/380}$ (Figure 4-2). Examining the $AI_{340/380}$ results, one can note that irradiance offsets lead to positive bias in UVAI and radiance offsets to negative biases. This is a more mixed result with respect to $AI_{354/388}$, this is likely due to the smaller spread in UVAI values for this pair. Because the UVAI is a ratio, the bias is small when there is an offset in both radiance and irradiance. This is true for both multiplicative or additive errors (see "Add_Both" and "Mul_Both" in Figure 4-2 and Figure 4-3). The error range and values are larger for $AI_{354/388}$ than for $AI_{340/380}$ as can be seen in the comparison in Figure 4-4.
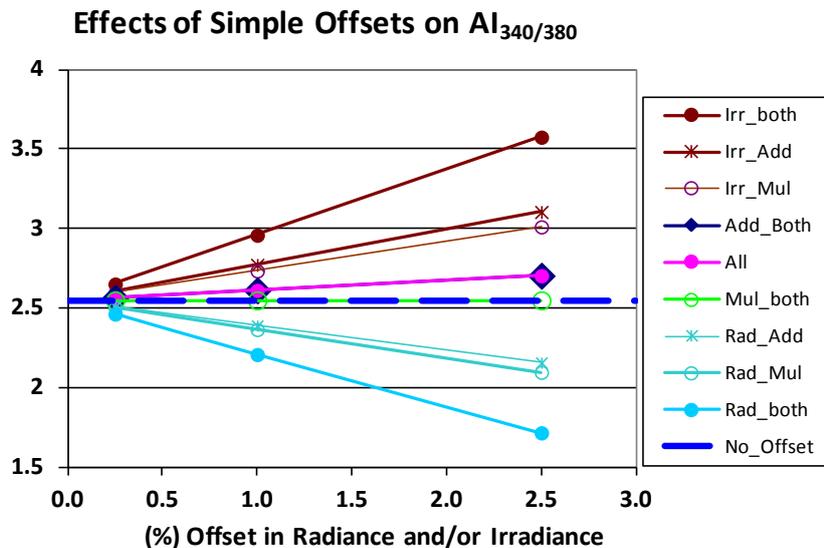

Figure 4-2. Effects on $AI_{340/380}$ from applying simple additive and/or multiplicative offsets in irradiance and/or radiance based on DISAMAR simulated UVAI. The percentage of offset is given on the x-axis, value of the UVAI on the y-axis and the different types of offsets are shown in different colors and line types and listed in the legend. The blue dashed line gives the UVAI value when no offsets are applied.
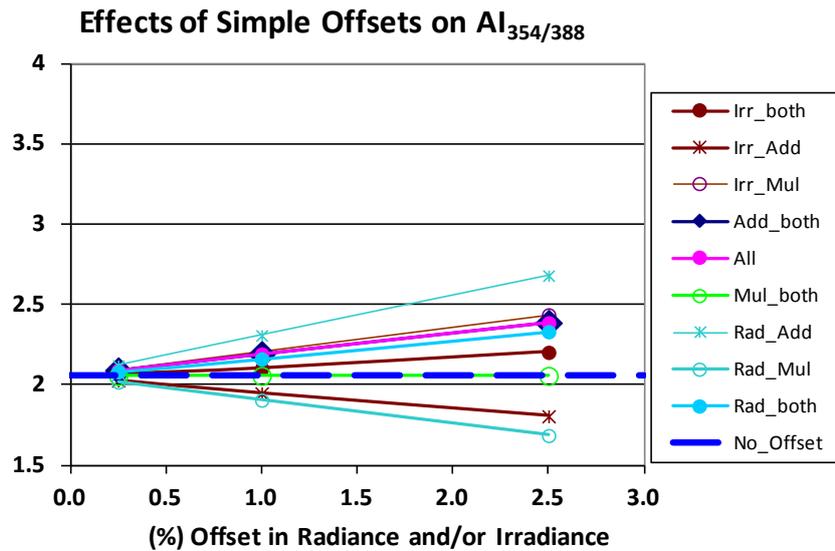
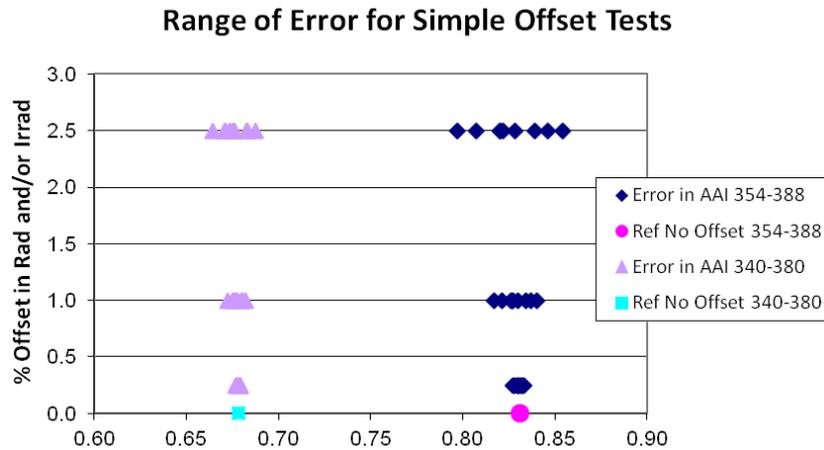Figure 4-3. Same as in Figure 4-2 but for $AI_{354/388}$.

Figure 4-4. Range of Error in UVAI on the x-axis versus the percent in offset on the y-axis for all simple offset tests shown in Figure 4-2 and Figure 4-3. $AI_{340/380}$ is shown in violet triangles and $AI_{354/388}$ is shown in blue diamonds, the reference error in UVAI with no offset is shown on the x-axis as a single character (light blue square for $AI_{340/380}$ and magenta circle for $AI_{354/388}$).

Figure 4-2 through Figure 4-4 illustrate that simple offsets are important sources for bias and error in the UVAI. Based on these simulated results, it is therefore recommended that the offsets in radiance and irradiance not be greater than 0.5%, with a goal of less than 0.25%.

4.4.2 Model errors

Errors in the UVAI are also dependent on knowledge of surface albedo and the wavelength-dependent variability of surface albedo. To test the latter the diagonals of the a priori surface albedo correlation matrix were varied between 0.999999 and 0.999000. It is notable that the latter value still represents a high degree of correlation. The effect on the error of UVAI resulting from a decrease in the degree of correlation is shown in Figure 4-5. As can be seen, the error increases rapidly with a decrease in the degree of correlation. The decrease in correlation leads to large errors in UVAI greater than 20 for both $AI_{340/380}$ and $AI_{354/388}$ when the a priori surface albedo correlation is reduced to 0.999000. It should also be noted that there is an offset between the two UVAIs where the $AI_{340/380}$ is roughly 0.5 higher than the $AI_{354/388}$. This reflects the difference in wavelength pair choice.
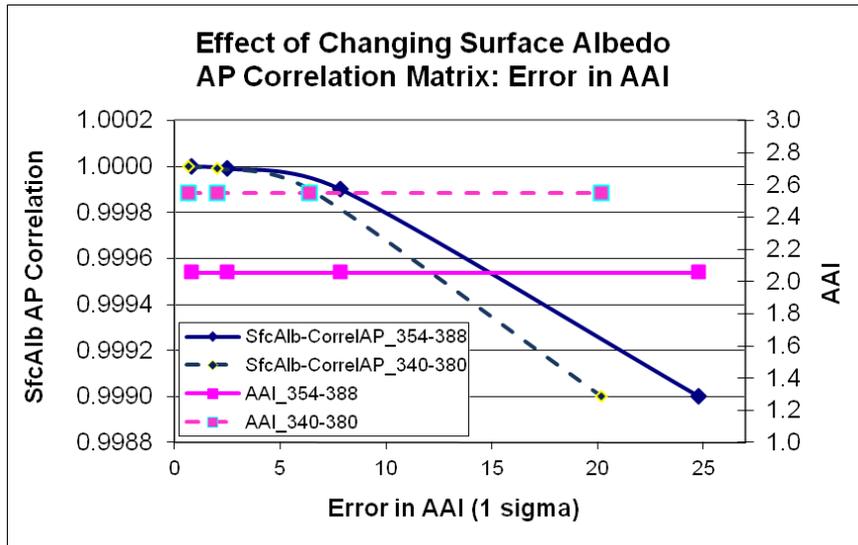
Figure 4-5. Effect in UVAI error as a result of changing the degree of correlation in the surface albedo a priori correlation matrix in DISAMAR for both AI$_{340/380}$ (dashed lines) and AI$_{354/388}$ (solid lines). Error in UVAI is on the x-axis, the value of the degree of correlation is shown by the blue lines and corresponds to the primary y-axis (left) and the value of the UVAI is shown in pink corresponding to the secondary y-axis (right).

As can be seen in Figure 4-5, the AI$_{354/388}$ is more sensitive to the degree of correlation as compared to AI$_{340/380}$. To investigate if correlations in actual surface albedo data are close to 1.0 between UVAI wavelengths, correlations were calculated for various OMI wavelengths using the Kleipool et al. (2008) OMI LER climatology database for 354 versus 388 nm and 342 versus 380 nm. It should be noted that 340 nm was not an available wavelength in the OMI LER climatology and so 342 nm was chosen as the closest alternative wavelength. Calculation of correlation coefficients are based on the following sample points: for a specific (lat-lon) cell in a given month, eight neighbor cells are also chosen, as well as cells for the preceding and following months. Thus, a single correlation coefficient is based on 9 grid cells for 3 months which equals a total of 27 sample points. Linear correlation coefficients have been calculated accordingly,

$$r = \frac{\sum((x_i - mx)*(y_i - my))}{\sqrt{\sum((x_i - mx)^2)*\sum(y_i - my)^2)}}$$ Eq. 4-8

where, x_i are LER values at the sample points for a specific wavelength and mx is the sample mean of x_i (likewise for y_i at the second wavelength); the summation (index i) is over the sample points. Here, r can take on values between -1 and 1. Using the neighbor cell and month scheme of calculating correlation dictates that correlations are much lower for highly inhomogeneous surfaces and for surfaces that change rapidly over time.
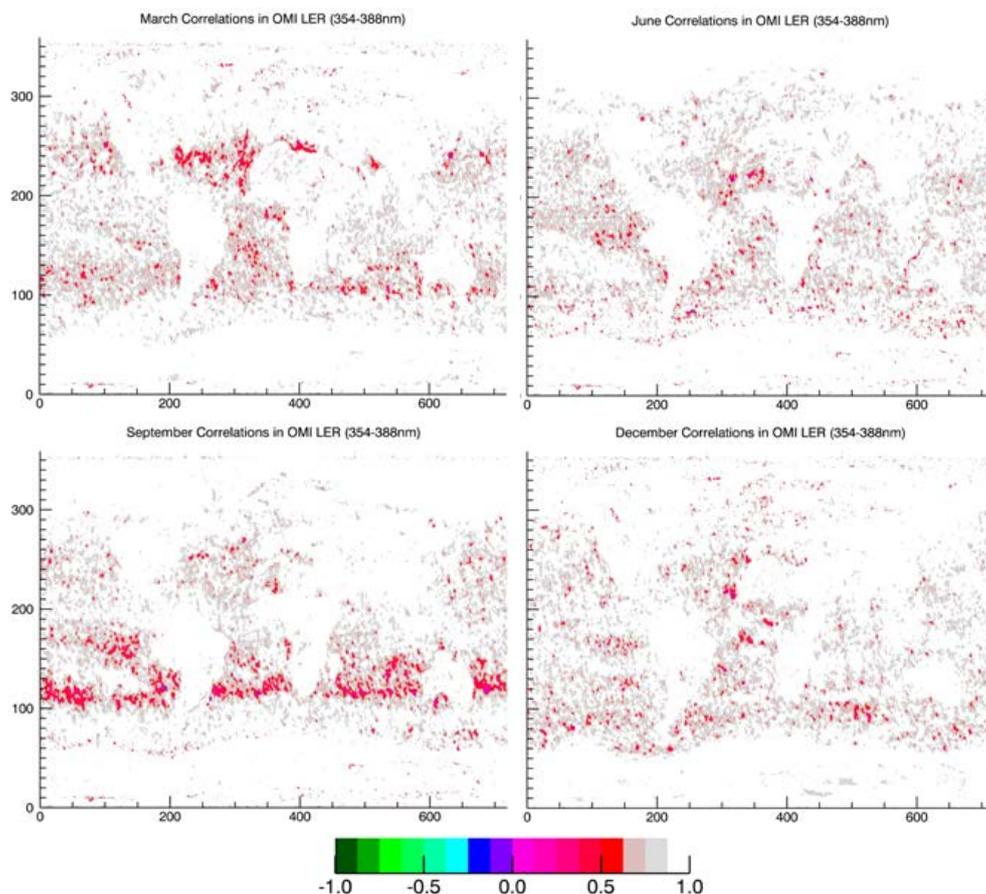
Figure 4-6. Seasonal variation in the correlation coefficients calculated for OMI LER between 354 and 388 nm based on the OMI LER database from Kleipool et al. (2008) for the following months: March (upper left), June (upper right), September (lower left), and December (lower right). Longitude and latitude indices are given on the x- and y-axes respectively. All values shown were found to be positive and greater than 0.5 which corresponds to the portion of the color scale farthest to the right where white and to a lesser extent, light gray colors represent the highest amount of positive correlation.

An example of the variation in surface albedo correlation for different months can be seen in Figure 4-2 based on the OMI LER climatology from Kleipool et al. (2008) for wavelengths relevant to $AI_{354/388}$. The correlations exhibit strong seasonal variability with the highest correlations over land surfaces as compared with lower values over ocean surfaces where there much less homogeneity. Based on evaluation of seasonal data from the Sea-viewing Wide Field-of-view Sensor (SeaWiFS), the highly variable patterns over ocean appear to be correlated with seasonal variations in ocean color. Correlations between OMI LER for the wavelengths relevant to $AI_{340/380}$ thus, 342 and 380 nm (not shown) are lower than those shown in Figure 4-2. In this case the higher sensitivity of $AI_{354/388}$ to the degree of correlation in surface albedo may be compensated by the fact that the surface albedo is better correlated at these wavelengths than those used by $AI_{340/380}$.

4.4.3   UVAI Sensitivities

In contrast to Sections 4.4.1 and 4.4.2 where errors in UVAI were presented, this section presents sensitivities or dependencies that the UVAI exhibits including aerosol type, height and optical thickness. UVAI has been simulated in DISAMAR for a wide range of surface types and aerosol types which can be viewed as representing a variety of the geophysical scenarios and is similar in method to the work presented by de Graaf et al. (2010). Variations in viewing geometry, surface albedo, τ_0, and ALH are summarized in Table 4-6 and were used as input for DISAMAR to calculate UVAI. The aerosol types and properties have been defined as a part of the ESA Aerosol-Climate Change Initiative project (De Leeuw et al., 2011) and include "dust", "sea salt", "weakly absorbing", "strongly absorbing". A fifth type of "moderately absorbing" aerosol type was added for this study and all properties of the aerosol types are summarized in Table 4-7.

As stated earlier, UVAI varies according to viewing geometry, aerosol layer properties including AOT, ALH, SSA and underlying surface albedo. Variation in UVAI as a function of τ_0, ALH and underlying surface albedo for a single layer of "strongly absorbing" aerosol particles (see Table 4-7) is shown in Figure 4-7. In this figure, it can be seen that the effects of surface albedo are strongest for aerosol layers with lower optical thickness and lower altitude. As optical thickness and layer height increase the effect is minimized. For aerosol layers with an optical thickness greater than 1.0 the layer height can be discerned if the surface albedo remains constant. For even thicker layers with an τ_0 greater than 2.0 the layer height can be discerned even if the surface albedo is inconsistent. This effect is dependent on how strongly absorbing the aerosol layer is and diminishes with increasing single scattering albedo of the aerosol layer. Simulations described in De Graaf et al., (2005) also describe the enhancement effect in AI values when strongly absorbing aerosol layers are located above clouds or other bright surfaces.

Table 4-6. Summary of AI simulations carried out for various geophysical scenarios.

Aerosol Type	VZA	SZA	RAA	Surface Albedo	AOT	Layer Height (Pa)	Total Number of Cases per λ-pair
Strongly, Moderately, and Weakly Absorbing	0, 30, 45, 60	0, 30, 45, 60, 75	0, 45, 90, 135, 180	0.0, 0.02, 0.05, 0.1, 0.2, 0.4, 0.8, 1.0	0.0, 0.1, 0.2, 0.5, 1.0, 2.0, 5.0	100000-90000, 90000-80000, 80000-70000, 70000-60000, 60000-50000	28000 28000 28000
Sea Salt	0, 30, 45, 60	0, 30, 45, 60, 75	0, 45, 90, 180	0.0, 0.02, 0.05, 0.1	0.1, 0.2, 0.5	100000-90000, 90000-80000	1920
Desert Dust	0, 30, 45	0, 30, 45, 60, 75	0, 45	0.02, 0.05, 0.1, 0.2	0.5, 1.0, 2.0	90000-80000, 80000-70000, 70000-60000	820

Table 4-7. Aerosol properties as defined by the Aerosol-CCI project* used in DISAMAR simulations.

| Aerosol Type	Refractive Index Real Part(550 nm)	Refractive Index Imag. Part(550 nm)	Eff. Radius (µm)	Geom. Std. Dev. (σ_i)	Variance (ln σ_i)	Geom. Mean Radius (µm)	Comments
Dust*	1.56(varies with wavelength)	0.0018 (varies with wavelength)	1.800	1.822	0.6	0.79	Non-spherical
Sea salt*	1.40	0.000	1.820	1.822	0.6	0.90	
Weakly absorbing*	1.40	0.003	0.142	1.7	0.53	0.07	SSA = 0.98 at 500nm
Strongly absorbing*	1.50	0.025	0.142	1.7	0.53	0.07	SSA = 0.80 at 500nm
Moderately absorbing	1.44	0.019	0.142	1.7	0.53	0.07	SSA = 0.89 at 500nm
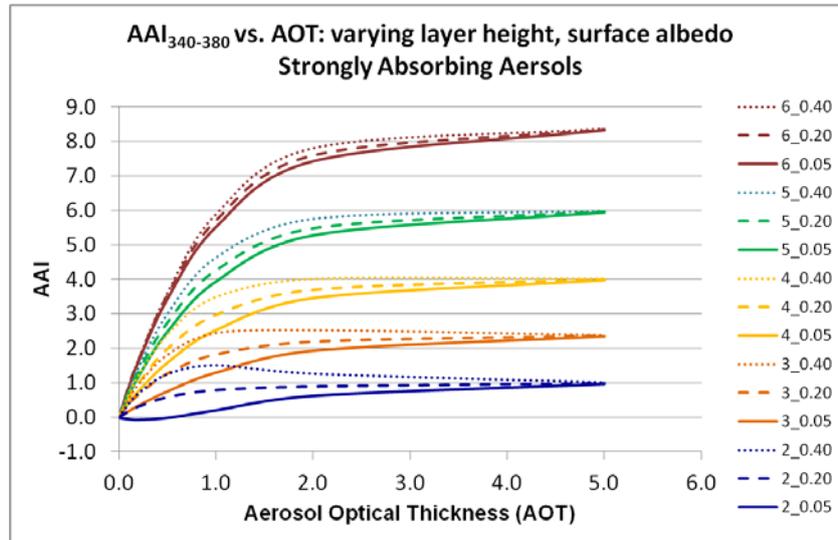
Figure 4-7. Variability of UVAI as a function of τ_0 for varying layer height and surface albedo. The legend depicts differing lines with labels consisting of a ALH index value followed by a surface albedo value. ALH indices correspond to varying colors as follows, 6 – 60000-50000 Pa (dark red), 5 – 70000-60000 Pa (green), 4 – 80000-70000 Pa (yellow), 3 – 90000-80000 Pa (orange), 2 – 100000-90000 Pa (blue). Differing line types correspond to surface albedo values: 0.40 (dotted), 0.20 (dashed), and 0.05 (solid). For this plot the viewing geometry was fixed (0° VZA, 30° SZA, 0° RAA).

A comparison of the behavior of UVAI as a function of τ_0 is given in Figure 4-8 for a fixed geophysical scenario for the five different aerosol types listed in Table 4-7 for both high and low layers. In this case the viewing geometry and the surface albedo are fixed so that the same values are used for each case. Figure 4-8 clearly illustrates that strongly and moderately absorbing aerosol types like those from dust and strongly absorbing particles like smoke lead to positive values in UVAI whereas, weakly absorbing and near-surface aerosol layers like sea salt or sulfates lead to near-zero and negative aerosol index values. Sea salt does not exist in high concentrations in elevated layers. As such, the results for sea salt are limited to low values of τ_0 and low layers in the atmosphere to reflect a more probable geophysical scenario.
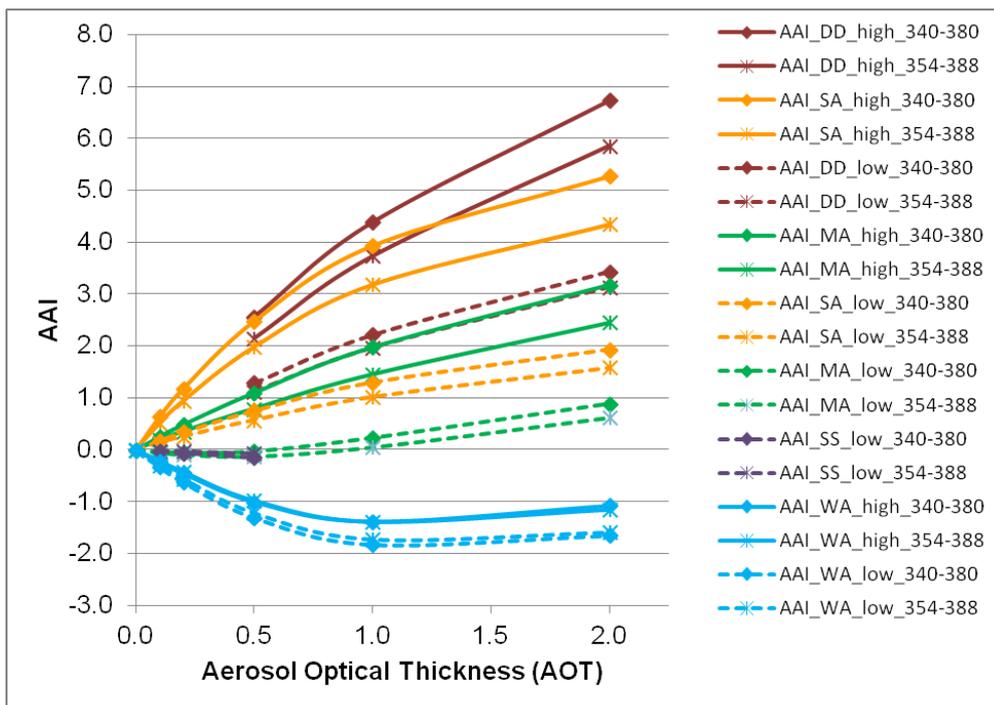
Figure 4-8. Variation of UVAI as a function of τ_0 for five different aerosols types (see Table 4-7) at two layer heights (high: 70000-60000 Pa (solid lines), low: 90000-80000 Pa (dashed lines)). Different colored lines are used for differing aerosol type (Desert Dust (DD) in dark red, Strongly Absorbing (SA) – orange, Moderately Absorbing (MA) in green, Sea Salt (SS) in purple, and Weakly Absorbing (WA) in light blue). Data marker shapes differ for wavelength pair (diamonds for $AI_{340/380}$ and stars for $AI_{354/388}$). For this plot the viewing geometry was fixed (0° VZA, 30° SZA, 0° RAA) as well as the surface albedo at 0.05.

4.4.4   Errors in UVAI related to ozone and NO_2 interference

The effects of ozone absorption in the UV cannot be ignored for some wavelengths used to calculate the UVAI. A comparison of the effect of improperly accounting for column ozone concentration for $AI_{340/380}$ and $AI_{354/388}$ is given in Figure 4-9. Ozone concentration was altered for the simulation of the UVAI using DISAMAR and held constant at 300 DU for the retrieval for both $AI_{340/380}$ and $AI_{354/388}$. The simulations have been carried out for a larger than expected range of variability in ozone concentration. The resulting bias in UVAI is shown in Figure 4-9 and is much greater for $AI_{340/380}$ than for $AI_{354/388}$ where the effect is nearly negligible. If ozone is known within 30 DU then the error in AI should be less than 3%.
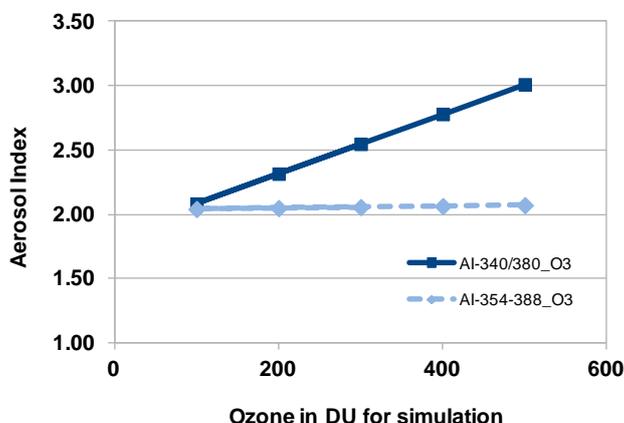

Figure 4-9. Bias in UVAI resulting from changing ozone concentration in simulation while fixing retrieval ozone concentration at 300 DU. $AI_{340/380}$ is shown as dark blue, solid line and $AI_{354/388}$ in light blue with dashed line.

The effect of unaccounted NO_2 concentrations were similarly tested in DISAMAR by varying concentrations typical of pristine to highly polluted environments (1×10^{15} molec/cm^2 to 2×10^{16} molec/cm^2). The effects on UVAI with increasing NO_2 concentration were negligible causing a decrease in UVAI value of 0.01 or less, where highest altitude aerosol layers exhibit a greater impact than lower altitude layers.

4.4.5   Effects of Clouds on UVAI

Several tests were carried out using DISAMAR to examine the effect of clouds on UVAI. The effect of clouds optically thick enough to shield underlying aerosol layers should also be considered and quantified. These tests were designed to establish a threshold at which absorbing aerosol can no longer be detected due to the masking effect of a cloud layer of varying cloud fraction located above an absorbing aerosol layer. A Lambertian cloud layer was used at two different heights above a strongly absorbing aerosol layer of constant AOT (2.0) at three different heights. Cloud fraction was varied from 0.0 to 1.0, where 1.0 is a fully clouded scene. As can be seen in Figure 4-10, for the highest altitude aerosol layer (dark blue line), absorbing aerosol is clearly detectable (as indicated by AI values of 1.0 and larger) up to a cloud fraction of 0.2. Lower altitude aerosol layers are marginally detectable at cloud fractions below 0.1 or less.
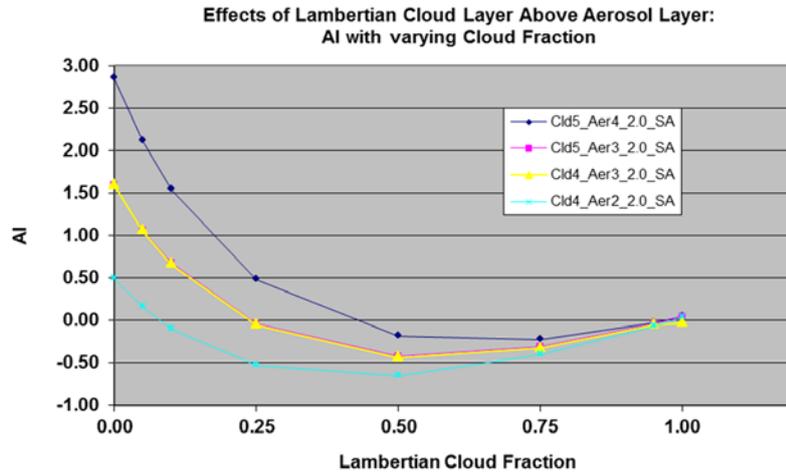
Figure 4-10. The effects on UVAI of a Lambertian cloud layer of variable cloud fraction located above a strongly absorbing aerosol layer with AOT = 2.0. Figure legend refers to varying aerosol (AerX) or cloud (CldX) layer where, X refers to a layer index as follows: layer extending from 100000-90000 Pa = 2, 90000-80000 Pa = 3, 80000-70000 Pa = 4, 70000-60000 Pa = 5.
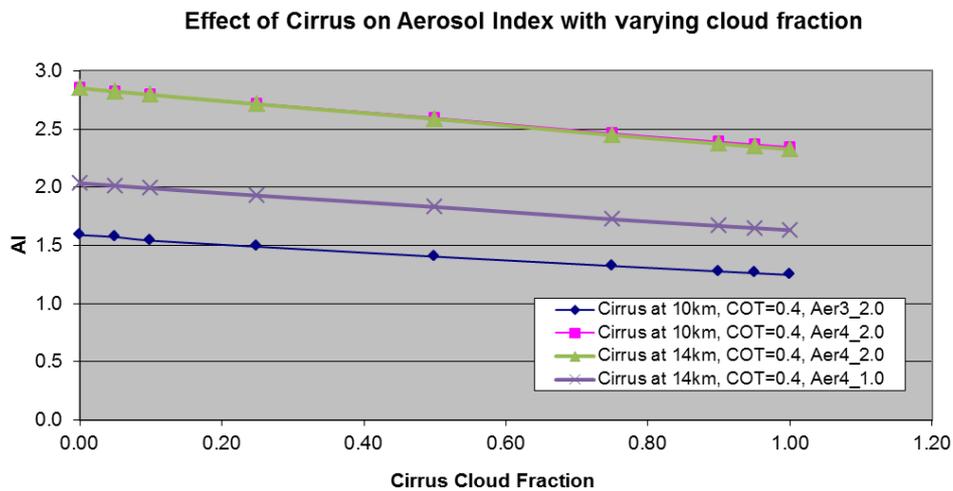

Figure 4-11. The effect on UVAI of cirrus layers at 10000 or 14000 m with varying cloud fraction located above a strongly absorbing aerosol layer. Cirrus properties are fixed and defined using HG parameters, including a cloud optical thickness of 0.4. Figure legend similar to Figure 4-10 where aerosol layer height is given by AerX and AOT was either 2.0 or 1.0 as listed in the legend.

The effect of cirrus cloud fraction on UVAI was also tested in DISAMAR using Henyey-Greenstein parameterization for cirrus properties. Cirrus properties were held constant and layers were tested at two heights, 10000 and 14000 m. Aerosol layers were tested at two different heights and with two AOTs (1.0 and 2.0). A layer of strongly absorbing aerosol (with varying AOT) was found to be detectable (AI value of 1.0 or larger) through cirrus layers at any cloud fraction as depicted in Figure 4-11. Also, the height of the cirrus layer appears, in this study to have little effect on the detection of absorbing aerosols.

4.4.6   Knowledge of terrain height for calculating UVAI

Tests using DISAMAR were carried out to define requirements for the knowledge of terrain height needed for calculation of UVAI, and to determine if resulting biases in UVAI are linear and to determine what vertical resolution is needed for terrain height data. To test this, the surface pressure used in DISAMAR was held constant at 101325 Pa for the simulation and varied in the retrieval calculation to values up to roughly 95000 Pa (see Table). These tests were carried out for a single strongly absorbing aerosol layer with varying height (layer between 35000-30000 Pa or 85000-80000

Pa) and optical thickness (0.2 or 0.5). The underlying surface albedo value was 0.05 and the variance of the surface pressure in the retrieval was set at 10000 Pa for all tests. Surface pressures tested and the corresponding altitudes are summarized in *Table 4-8* below. The UVAI values and resulting biases are shown in Figure 4-12 for an upper and lower tropospheric aerosol layer using the 340/380 nm and 354/388 nm wavelength pairs. The results indicate that errors in the assigned terrain height less than 250 m result in UVAI bias of approximately 0.3 depending in layer height and thickness, thus it is recommended that a vertical resolution of 250 m is acceptable for calculation of the UVAI.

Table 4-8. Summary of pressures biases tested and corresponding altitudes.

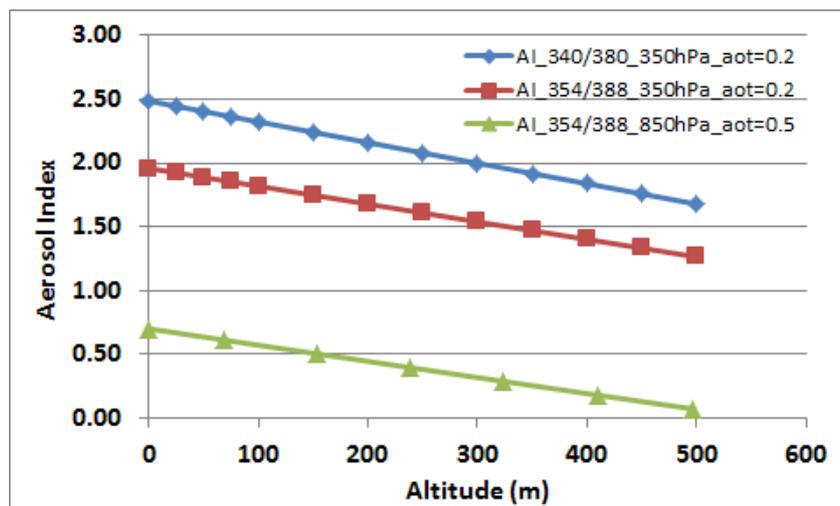| Pressure (Pa)	Altitude (m)
101325	0
101025	25
100725	50
100427	75
100129	100
99535	150
98944	200
98355	250
97771	300
97189	350
96609	400
96033	450
95459	500

Figure 4-12. UVAI values resulting from varying terrain altitude in simulation and retrieval, illustrating resultant bias in UVAI based on knowledge of terrain height for varying aerosol layer height and optical thickness.

4.4.7   Other points of consideration for using UVAI datasets

While these issues are not considered errors as such, it is important for data users to consider the effects of ocean color, sun glint, and extreme viewing angles. It is difficult to fully quantify the effects of variations in ocean color, sediment, gelbstof and clear water as studies of the optical properties of ocean have not been carried at wavelengths short enough for the AI. However, variations in these ocean parameters often lead to positive AI values over remote ocean regions where no absorbing aerosol is expected to be present. Similarly, AI has higher than expected values due to sun glint and at extreme viewing angles (the latter is described in detail in de Graaf et al., 2005). As such the AI, which will be calculated for all pixels, should be screened for sun glint. Experience from using the OMI AI indicates that values of UVAI at large solar zenith angles (greater than 60°) and at swath edges should be used with care as shown in Penning-de Vries, 2014.

4.5   Conclusions

The well-proven methods for calculation of the AI used by OMI, based on the heritage of TOMS and following instruments, will be continued. Slight modifications, like enhancing the LUT used for storing Rayleigh reflectance, should help to improve the TROPOMI UVAI but ensure that it can and will be used to extend the existing long-term data record of AI. The increased spatial resolution of TROPOMI as compared to OMI will yield a data product capable of detecting episodic smoke and dust events on a much finer spatial scale. TROPOMI UVAI will be calculated using the classical heritage pair of 340/380 nm, but based on results of error and model analyses also continue the record of AI at the OMI chosen 354/388 nm wavelength. The low computational demands of the UVAI should allow for feasible maintenance of both $AI_{340/380}$ and $AI_{354/388}$. Based a series of tests carried out using DISAMAR, UVAI performs well for a wide range of geophysical scenarios as long as errors such as simple additive or multiplicative errors in the radiance or irradiance are minimized and the surface albedo is well correlated at both wavelengths of a given pair.

5   Validation of UV aerosol index

Validation can be carried out in several classical ways using ground-based instruments and instrument networks, in-situ measurement campaigns designed to address specific algorithm features, satellite intercomparisons, and by developing specific (software) tools.

Validation of the UVAI cannot be carried out in a traditional way because it is not a physical quantity and depends upon too many different parameters. However, tests to evaluate the performance of AI can be carried out in several ways. One of the ways to quasi-validate the UVAI is to intercompare TROPOMI UVAI to concurrent data sets including OMI, GOME-2, and OMPS. OMI and OMPS are ideal for comparison since they both have afternoon overpass times. Comparing different AI data sets along with simulated AI can point to reasons why discrepancies and offsets arise between data sets due to differences in calibration, instrument characteristics and other factors. UVAI consists of a range of negative and positive values typically between -2 and +2, and only a small percentage of global area is covered by strongly absorbing aerosols at any given time. Regional analyses in areas of known absorbing aerosol sources like biomass burning or desert dust outflow regions are also useful to see if expected seasonal cycles are captured in the AI data. Here, these averages over more localized source regions should be positive.

One classic validation tool for aerosol data products is the AERONET measuring network of sun photometers. However, this cannot be used to compare with UVAI because the sun photometers measure attenuated rather than backscattered light and the UVAI relies on the interaction between Rayleigh scattering and absorption due to the presence of aerosols. Airborne spectrometers covering the UV spectral range are however a good alternative as long as they measure at sufficiently high altitude. The Airborne Compact Atmospheric Mapper (ACAM) is an example of such an airborne spectrometer. This instrument was designed and built at the NASA Goddard Space Flight Center as part of an effort to provide cost-effective remote sensing observations of tropospheric and boundary layer pollutants and visible imagery for cloud and surface information (Kowalewski and Janz, 2009). It consists of two crossed Czerny-Turner miniature spectrometers. The first measures in the spectral range from 310 nm to 520 nm at 0.8 nm spectral resolution and is optimized for tropospheric pollutants and water vapor but could also be used to calculate UVAI. The second spectrometer measures from 460 nm to 900 nm at 1.7 nm spectral resolution and is optimized for ocean color, water vapor, and aerosols and could be potentially used to measure Aerosol Layer Height in situ. Flights using this instrument could be used for validation of UVAI and/or ALH if timed to be adequately close to the expected TROPOMI overpass time.

6   General conclusion and outlook

The TROPOMI UV aerosol index will add to the heritage of more than 30 years of data describing the presence of aerosol with daily, global coverage. The TROPOMI UVAI product will provide information for aerosol correction in trace gas retrievals as well as critical near real-time information for tracking episodic aerosol events like volcanic eruptions, dust outbreaks, and biomass burning events. When used in combination with the TROPOMI ALH and results from modeling studies, the UVAI can be used to describe aerosol layer characteristics in a more quantitative manner. By calculating the UVAI at two wavelength pairs TROPOMI will provide the chance to better combine datasets into long-term records and to critically intercompare among concurrent measurements thus facilitating the evaluation of long-term trends and description of inter-satellite measurement differences.

7   References

Chiapello, I., Prospero, M., Herman, J.R., and Hsu, C. (1999). Detection of mineral dust over the North Atlantic Ocean and Africa with the Nimbus 7 TOMS. *Journal of Geophysical Research*, 104(D8): 9277-9291.

Dave, J.V., and Mateer, C.L. (1967). A preliminary study on the possibility of estimating total atmospheric ozone from satellite measurements. *Journal of Atmospheric Sciences*, 24: 414–427.

De Graaf, M. and Stammes, P. (2005). SCIAMACHY Absorbing Aerosol Index—calibration issues and global results from 2002-2004. *Atmospheric Chemistry and Physics*, 5: 2385-2394.

De Graaf, M., Stammes, P., Torres, O., and Koelemeijer, R.B.A. (2005). Absorbing Aerosol Index: Sensitivity analysis, application to GOME and comparison to TOMS. *Journal of Geophysical Research*, 110(D01201). doi:10.1029/2004JD005178

De Graaf, M., Tuinder, O., and Tilstra, G. (2010). O3MSAF Algorithm Theoretical Basis Document for ARS. KNMI ATBD, Ref OM3SAF/KNMI/ATBD/002, issue: 1.0, date: 2010-04-29.

De Haan, J.F, Bosma, P.B., and Hovenier, J.W. (1987). The adding method for multiple scattering calculations of polarized light. *Astronomy and Astrophysics*, 183: 371–391.

De Leeuw, G., Kinne, S., Veefkind, P., Holzer-Popp, T., Stein-Zweers, D., Tanré, D., Thomas, G., North, P., Dubovik, O., and Kokhanovsky, A. (2011). ESA Aerosol-CCI Technical Note: Aerosol Models, issue: 1.1, date: 2011-09-06.

Dubovik, O., Holben, B., Eck, T.F., Smirnov, A., Kaufman, Y.J., King, M.D., Tanré, D., and Slutsker, I. (2002). Variability of absorption and optical properties of key aerosol types observed in worldwide locations. *Journal of the Atmospheric Sciences*, 59: 590–608.

Herman, J.R., Bhartia, P.K., Torres, O., Hsu, C., Seftor, C., and Celarier, E. (1997). Global distribution of UV-absorbing aerosols from Nimbus 7/TOMS data. *Journal of Geophysical Research*, 102(D14): 16,911–16,922. doi:10.1029/96JD03680

Hsu, N.C., Herman, J.R., Bhartia, P.K., Seftor, C.J., Torres, O., Thompson, A.M., Gleason, J.F., Eck, T.F., and Holben, B.N. (1996). Detection of biomass burning smoke from TOMS measurements. *Geophysical Research Letters*, 23(7): 745-748.

Hsu, N.C., Herman, J.R., Torres, O., Holben, B.N., Tanre, D., Eck, T.F., Smirnov, A., Chatenet, B., and Lavenu, F. (1999). Comparisons of the TOMS aerosol index with Sun-photometer aerosol optical thickness: Results and applications. *Journal of Geophysical Research*, 104(D6): 6269–6279.

Ingmann, P., Veihelmann, B., Langen, J., Lamarre, D., Stark, H., and Bazalgette Courrèges-Lacoste, G. (2012). Requirements for the GMES Atmosphere Service and ESA's implementation concept: Sentinels-4/5 and -5p. *Remote Sensing of Environment*, 120: 58–69. doi:10.1016/j.rse.2012.01.023

Kleipool, Q.L., Dobber, M.R., De Haan, J.F., and Levelt, P.F. (2008). Earth surface reflectance climatology from 3 years of OMI data. *Journal of Geophysical Research*, 113(D18308):22 pp. doi:10.1029/2008JD010290

Koelemeijer, R.B.A., Stammes, P., Hovenier, J.W., and De Haan, J.F. (2001). A fast method for retrieval of cloud parameters using oxygen A band measurements from the Global Ozone Monitoring Experiment. *Journal of Geophysical Research*, 106(D4): 3475–3490.

Koelemeijer, R.B.A., De Haan, J.F., and Stammes, P. (2003). A database of spectral surface reflectivity in the range 335–772 nm derived from 5.5 years of GOME observations. *Journal of Geophysical Research*, 108(D24070):13 pp.

Kowalewski, M.G., and Janz, S.J. (2009). Remote sensing capabilities of the Airborne Compact Atmospheric Mapper. In J. Butler, X. Xiong, X. Gu (Eds.), Earth Observing Systems XIV: Proceedings of SPIE Vol. 7452, 74520Q.

Krotkov, N. A., Torres, O., Seftor, C., Krueger, A. J., Kostinski, A., Rose, W. I., Bluth, G. J. S., Schneider, D. J., & Shaefer, S. J. (1999). Comparison of TOMS and AVHRR volcanic ash retrievals from the August 1992 eruption of Mount Spurr. Geophysical Research Letters, 26: 455– 458.

Penning de Vries, M.J.M., Beirle, S., and Wagner, T. (2009). UV Aerosol Indices from SCIAMACHY: introducing the SCattering Index (SCI). *Atmospheric Chemistry and Physics*, 9: 9555–9567. doi:10.5194/acp-9-9555-2009

Penning de Vries, M. J. M., Dörner, S., Puķīte, J., Hörmann, C., Fromm, M. D., and Wagner, T. (2014). Characterisation of a stratospheric sulfate plume from the Nabro volcano using a combination of passive satellite measurements in nadir and limb geometry. *Atmospheric Chemistry and Physics*, 14: 8149-8163, doi:10.5194/acp-14-8149-2014

Tilstra, L.G., de Graaf, M., Aben, I., and Stammes, P. (2012). In-flight degradation correction of SCIAMACHY UV reflectances and Absorbing Aerosol Index. *Journal of Geophysical Research*, 117(D06209). doi:10.1029/2011JD016957

Torres, O., Bhartia, P.K., Herman, J.R., Ahmad, Z., and Gleason, J. (1998). Derivation of aerosol properties from satellite measurements of backscattered ultraviolet radiation: Theoretical basis. *Journal of Geophysical Research*, 103(D14): 17,099–17,110. doi:10.1029/98JD00900

Veefkind, J.P., Aben, I., McMullan, K., Förster, H., De Vries, J., Otter, G., Claas, J., Eskes, H.J., De Haan, J.F., Kleipool, Q., Van Weele, M., Hasekamp, O., Hoogeveen, R., Landgraf, J., Snel, R., Tol, P., Ingmann, P., Voors, R., Kruizinga, B., Vink, R., Visser, H., and Levelt, P.F. (2012). TROPOMI on the ESA Sentinel-5 Precursor: A GMES mission for global observations of the atmospheric composition for climate, air quality and ozone layer applications. *Remote Sensing of Environment*, 120: 70–83. doi:10.1016/j.rse.2011.09.027

Wang, P., Tuinder, O.N.E., Tilstra, L.G., and Stammes, P. (2012). Interpretation of FRESCO cloud retrievals in case of absorbing aerosol events. *Atmospheric Chemistry and Physics*, 12: 9057–9077. doi:10.5194/acp-12-9057-2012

Appendix

The lookup table for UVAI calculation is stored in a NetCDF-4 file. Support dimensions are included in the file to ensure the data is interpreted correctly.

Name	Length	Description
wavelengths	4	The 4 wavelengths, for both pairs.
altitudes	37	The vertical grid (250 m intervals)
o3_columns	8	Total vertical column axis
no2_columns	1	Total column value for NO2
mu0	42	Cosine of solar zenith angle
mu	42	Cosine of viewing zenith angle
fourier	3	Fourier coefficient
spherical_albedo	wavelengths, altitudes, o3_columns	$S(\lambda)$
transmission_matrix	wavelengths, altitudes, o3_columns, mu, mu0	$T(\lambda)$
reflectance_0	wavelengths, altitudes, o3_columns, mu, mu0, fourier	$R_{a}(\lambda)$

Instead of interpolation in the azimuth direction, a Fourier series of length 3 is used. This provides an exact solution in case of Rayleigh scattering, as is the case here. Note that this LUT is identical to the lookup tables used for GOME-2 and SCIAMACHY aerosol indices, down to the same radiative transfer code. The only change is the increased number of surface elevations, from 1000 m intervals to 250 m intervals. This LUT is further described in [RD08].